Journal of Power Sources 184 (2008) 212–219

Contents lists available at ScienceDirect

Journal of Power Sources

journal homepage: www.elsevier.com/locate/jpowsour

Analysis of flooding as a stochastic process in polymer electrolyte membrane (PEM) fuel cells by impedance techniques

Sunil K. Roy, Mark E. Orazem*

Department of Chemical Engineering, University of Florida, Gainesville, FL 32611, USA

ARTICLE INFO

Article history:
Received 24 April 2008
Received in revised form 2 June 2008
Accepted 4 June 2008
Available online 14 June 2008

Keywords:
PEM fuel cells
Impedance spectroscopy
Flooding
Drying
Measurement model
Stochastic error

ABSTRACT

Impedance measurements were conducted to gain insight into flooding of a single polymer electrolyte membrane (PEM) fuel cell. The stochastic character of the formation of water droplets and subsequent removal by gas flow is demonstrated to increase the standard deviation of impedance measurements, yielding a sensitive manner to detect onset of flooding. The increase in stochastic noise associated with flooding was more apparent at low frequencies, due to the closer match to the characteristic frequency associated with the growth and removal of water droplets. The onset of flooding was sensitive to the design of the gas diffusion layer.

1. Introduction

The performance of the fuel cell is influenced by kinetic limitations at low current densities, Ohmic limitations at intermediate current densities, and mass-transfer limitations at high current densities. Kulikovsky [1] and Berg et al. [2] have described in detail the critical role of water management in operation of the fuel cell. To maintain proton conductivity, the fuel cell membrane must remain hydrated. To achieve hydration, the relative humidity of inlet gasses is typically held at a large value. Water, however, is also a product of the cathodic reaction; thus, an excess of water in the cathode is commonly observed, which can lead to condensation and subsequent flooding. Flooding increases the resistance associated with the gas diffusion layer and may even block flow channels, reducing the availability of oxygen [3]. Condensed water may be removed by gas flow. Thus, changes in design of reactant flow channels and gas diffusion layers have been proposed to reduce the influence of flooding.

A comprehensive review of the methods used to directly measure the presence of liquid water during the fuel cell operations was provided by St-Pierre [4]. Pressure drop has been reported to provide a suitable diagnostic tool for monitoring flooding in the fuel cell [5]. Flooding was also investigated by correlating the appearance of flooding to the Faradaic resistance [6]. Barbir et al. [7] have investigated the relationship between pressure drop and cell resistance to make a distinction between flooding and drying. They observed that both pressure drop and cell resistance changed in case of drying; whereas, only pressure drop changed under flooding conditions. Ge et al. [8] observed that the anode flooding is mainly due to water-droplet condensation at channel walls in contrast to flooding at the cathode which is usually attributed to condensation in gas diffusion layer (GDL). They have also reported that use of a hydrophilic GDL and elevated anode plate temperature could mitigate anode flooding. The onset of flooding may be seen in steady-state measurements, but the impedance response is even more sensitive to appearance of flooding conditions. The impedance technique has recently been used to detect membrane drying, flooding, and anode poisoning of fuel cell stacks [9]. Merida et al. [10] have also investigated failure modes (drying and flooding) of the fuel cell using the impedance technique. The approach taken by LeCanut et al. [9] and Merida et al. [10] was to detect flooding by observing increases in the value of the impedance as compared to a normal impedance measured at the beginning of cell operation. The advantage of their approach is that a physical model is not needed. The difficulties with normalizing the impedance to the impedance measured at the beginning of cell operation are that steady-state operation will generally not be established during this measurement, that there may be other reasons for increases in cell impedance with time, and that flooding may already be taking place during the initial measurement.

* Corresponding author. Tel.: +1 352 392 6207; fax: +1 352 392 9513.
E-mail address: meo@che.ufl.edu (M.E. Orazem).

0378-7753/$ – see front matter © 2008 Elsevier B.V. All rights reserved.
doi:10.1016/j.jpowsour.2008.06.014

Locally resolved impedance spectroscopy and NMR imaging have been used to investigate flooding and drying in the fuel cell by Schneider et al. [11–13]. The authors reported that, for co-flow configurations, membrane drying was evident near the gas inlet and flooding was severe near the gas outlet [12]. The authors have also reported that drying and flooding were more pronounced in co-flow as compared to counter-flow configurations [13]. Fouquet et al. [14] fitted a Randles-like equivalent circuit to impedance data and correlated circuit values to the state-of-health (flooding and drying) of the fuel cell. The Randles-like circuit, however, cannot account for all the phenomena taking place in the fuel cell. While there are differences in the specific approaches taken, the underlying concept for each of these approaches was that one can detect flooding by observing increases in the value of the impedance.

The object of the present work was to explore how the stochastic character of flooding can be exploited to improve sensitive of impedance spectroscopy to detect onset of flooding. Impedance measurements were performed as a function of different parameters such as current density, temperature, back pressure, and time. A model for base-level noise in impedance measurements for normal conditions (non-flooded) was developed using a measurement model analysis [15–19], and stochastic errors were also assessed by transient fixed-frequency measurements. A comparison of the actual noise to the base-level noise was used to detect onset of flooding. A preliminary version of this concept was described by Roy and Orazem [20].

2. Experimental

The experimental system and the impedance instrumentation used are presented in this section.

2.1. Materials and chemicals

The membrane electrode assembly (MEA) (purchased from Ion Power Inc., New Castle, DE) employed 0.0508 mm (2×10^{-3} in.) thick Nafion N112 with catalyst layers of about 0.025 mm on both sides of the membrane. The active surface area was 5 cm^2. The catalyst layers were platinum supported on carbon with a Pt catalyst loading of 0.4 mg cm^{-2} on both the anode and the cathode sides. Two types of gas diffusion layers (GDL) were used during assembly of the MEA. Both have an effective thickness of 0.284 mm and were made of carbon cloth, but one was uniformly macro-porous while the other had variable porosity. The non-uniform GDL was micro-porous to the catalyst side and macro-porous to the channel side. Similar GDL structures have been reported in the literature [21–23]. The material of the interdigitated flow channel used was graphite with the outlet lower than the inlet to facilitate removal of condensed water. A torque of 45 in.-pounds was applied to the fuel cell assembly. Hydrogen gas was used as fuel and a 79% N_2 and 21% O_2 mixture was used as oxidant. Compressed N_2 was used to purge the fuel cell before and after experiments. A Barnstead E-Pure Water System with an ion resistivity of 14.9 MΩ cm was used as a source of deionized water delivered to the anode and the cathode humidifiers.

An 850C fuel-cell test station (supplied by Scribner Associates, Southern Pines, NC) was used to control reactant flowrates and temperatures. The test station was connected to a computer by an interface for data acquisition. The gas flows were humidified to 100% relative humidity at the respective temperatures. The hydrogen flow rate was 0.1 l min^{-1} and the air flow rate was 0.5 l min^{-1}. The maximum stoichiometry for hydrogen and air was 1.5 and 2.5, respectively and the cell was operated at the fully humidified condition.

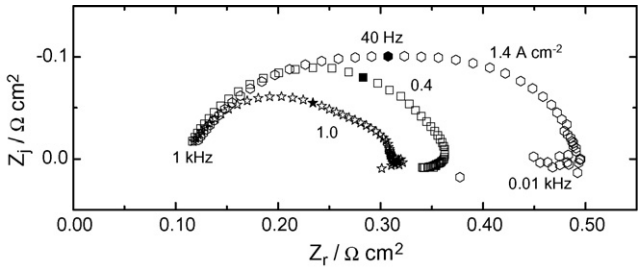

Fig. 1. Impedance data recorded with the 850C with applied current density as a parameter. The anode, cathode, and cell temperatures were set to 50 °C.

2.2. Electrochemical impedance measurements

Impedance measurements were performed using two different systems. The 850C fuel-cell test station contains an electronic load and frequency response analyzer. All electrochemical measurements were performed with a two-electrode cell. The anode was used as a pseudo-reference electrode. The impedance measurements were conducted in galvanostatic mode for frequency range of 10 kHz to 5 mHz with a 10 mA peak-to-peak sinusoidal perturbation. Lissajous plots were used to confirm that the perturbation amplitude was low enough to achieve a linear response. The corresponding potential perturbation ranged from 0.04 to 0.4 mV. The frequencies were spaced in logarithmic progression with 10 points per frequency decade. Impedance scans were conducted in auto-integration mode with a minimum of 2 cycles per frequency measured.

3. Results

The influence of flooding on the operation of the fuel cell was investigated using impedance spectroscopy. The results of frequency scan and single-frequency time-dependent measurements are presented in following sections.

3.1. Impedance response

A typical impedance response is presented in Fig. 1 with current density as a parameter. The size of the intermediate-frequency and the low-frequency arcs increased with increasing current density, an effect which was suggested in the literature [9,14] to be due partially to flooding. The impedance spectra were relatively smooth for low-current densities; however, the spectra have significant scatter at higher current densities where flooding was probable. The scatter was particularly evident at low frequency, where the spectra show jumps in value which may be associated with removal of condensed water. Similar results were observed at other temperatures. The impedance measured at 70 ° C is presented in Fig. 2 with

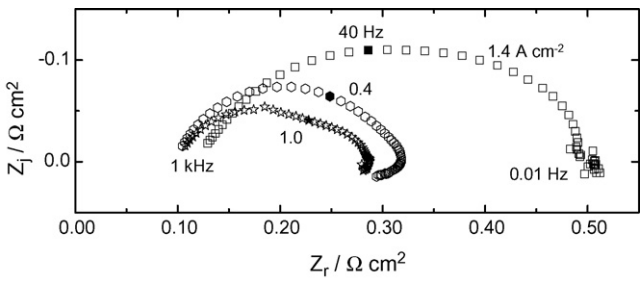

Fig. 2. Impedance data recorded with the 850C with applied current density as a parameter. The anode, cathode, and cell temperatures were set to 70 °C.

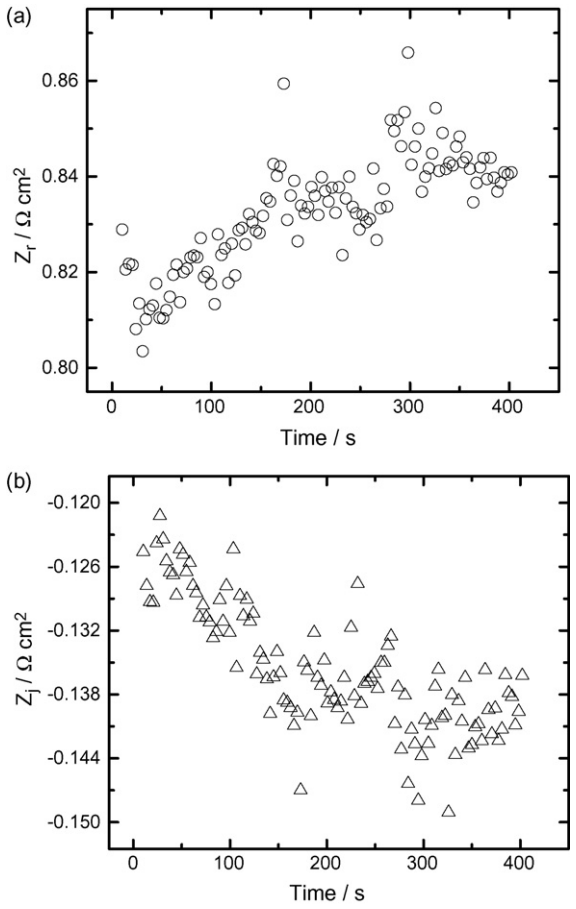

Fig. 3. Single-frequency impedance measurements recorded at 0.1 Hz, 70 °C, and 1.4 A cm^{-2} as functions of time: (a) real part; (b) imaginary part.

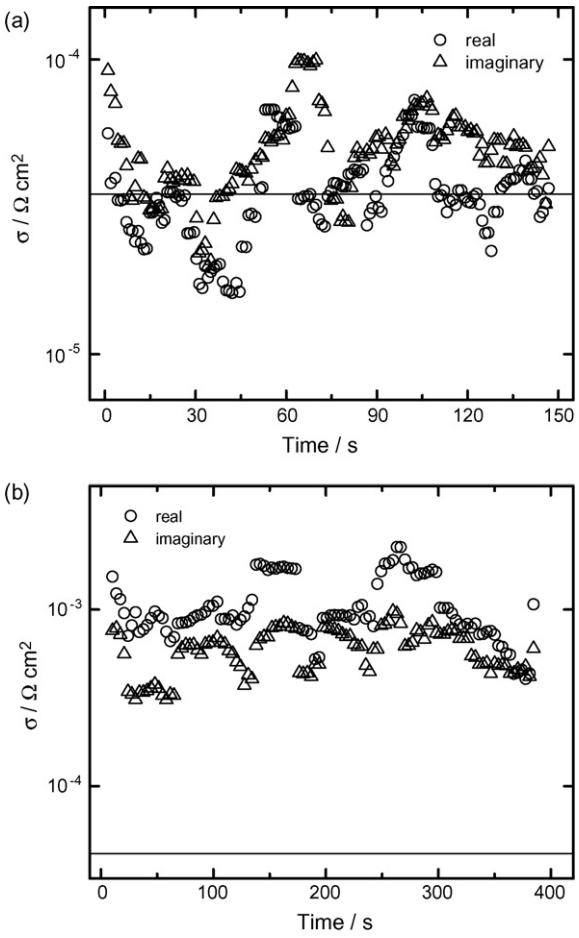

Fig. 4. The standard deviation of the single-frequency impedance measurements recorded at 1.4 A cm^{-2} and 70 ° C as functions of time: (a) at a frequency of 100 Hz; (b) at a frequency of 1 Hz (as presented in Fig. 3). The solid line represents the empirical model developed for the error structure given by Eq. (1).

current density as a parameter. Here also the impedance data have greater degree of scatter at higher current densities, and this scatter is particularly evident at lower frequencies.

3.2. Stochastic error in impedance response

The standard deviations of the stochastic errors were estimated from both impedance spectra and single-frequency transients for dry, flooded, and non-flooded conditions.

3.2.1. Sensitivity to flooding

The impedance was recorded as a function of time for different current densities and fixed-frequencies. For example, the real and imaginary parts of impedance at 0.1 Hz and 1.4 A cm^{-2} are presented as functions of time in Fig. 3 (a) and (b), respectively. The standard deviations in the impedance data were calculated using a moving average method to account for the systematic changes shown in Fig. 3. The standard deviations for the real and imaginary parts of the impedance response are presented in Fig. 4(a) for a measured frequency of 100 Hz and in Fig. 4(b) for a frequency of 1 Hz. At low frequencies, Fig. 4(b), the standard deviation of the real part of the impedance is clearly larger than that of the imaginary part. The solid line given in Fig. 4 represents the model value for the standard deviation, developed in a subsequent section for non-flooded conditions.

The standard deviations for the real part of the impedance are presented as a function of current density in Fig. 5 for frequencies of 0.1, 1, and 100 Hz. The stochastic errors in the impedance increased with increasing current density, in particular for the lower frequencies of 0.1 and 1 Hz. The standard deviation at lower frequencies are higher than that at higher frequencies for any given current density.

The statistical nature of the error structure may be used to explain the larger standard deviation observed at larger current densities. As shown in Fig. 4(b), the standard deviation of the real part of the impedance at 1 Hz was much higher as compared to

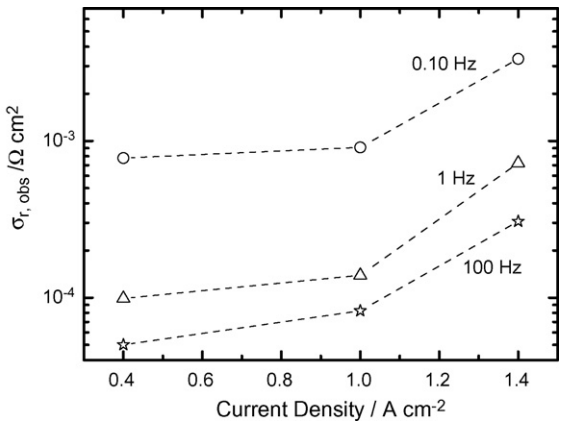

Fig. 5. The standard deviations for the real part of the impedance as a function of current density with frequency as a parameter for cell operation at 70 °C.

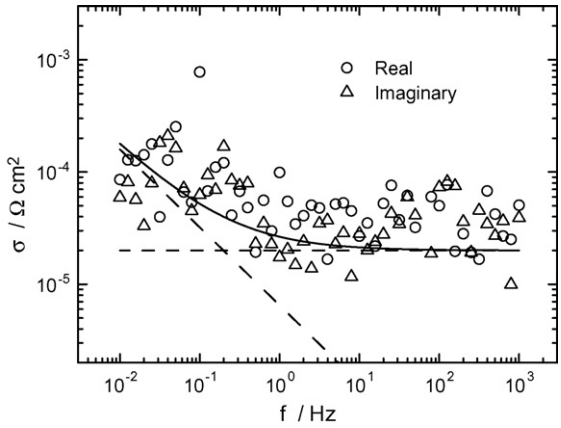

Fig. 6. Standard deviations for the impedance data obtained at a current density of 0.4 A cm^{-2}. The solid line represents the empirical model developed for the error structure given by Eq. (1). The dashed lines represent the asymptotic behavior of the model at high and low frequencies.

imaginary part. The results presented in Fig. 4(a) indicate that at 100 Hz, the standard deviation of real and imaginary parts of the impedance were also unequal, but the imaginary part of the impedance seems to have the larger standard deviation. For causal systems which satisfy the Kramers-Kronig relations, the standard deviation in the real and imaginary parts should be equal [24]. The literature indicates that, at low frequencies, the real part of the impedance is more sensitive to flooding [9,10]; therefore, the higher standard deviation of the real part of the impedance observed at low frequencies may be attributed to onset of flooding.

3.2.2. Baseline error structure

To establish a baseline error-structure model for the standard deviation of impedance measurements in the absence of flooding, a measurement model analysis [15–17,19] was applied to a large set of replicated impedance data. The measurement model was used to filter small systematic changes from one measurement to the other. The standard deviations for impedance response recorded at 0.4 A cm^{-2}, presented in Fig. 6, were smaller than those observed at both larger and at smaller current densities. The real and imaginary parts of the impedance were statistically indistinguishable at all frequencies, in agreement with expectations for data that are consistent with the Kramers-Kronig relations.

The model for error structure developed in previous work for a broad variety of electrochemical and electronic systems [25,26] did not provide a good representation of the error structure presented in Fig. 6. The failure of the general model to apply to the present data was attributed to differences in the parameters used to make the measurement. An empirical model was found to follow the form:

$$\sigma_r = \sigma_j = c + |Z_{r,\max}|(af^{-b}) \tag{1}$$

where $a = 9 \times 10^{-5}$, $b = 0.695$, and $c = 3.5 \times 10^{-5}$. The model can be rationalized by examination of the standard formula for propagation of stochastic errors, which can be written for impedance as

$$\sigma_Z^2 \cong \sigma_I^2 \left[\frac{\partial Z}{\partial \Delta I}\right]^2 + \sigma_V^2 \left[\frac{\partial Z}{\partial \Delta V}\right]^2 \tag{2}$$

where ΔI and ΔV are perturbations in current and potential, respectively, and Z is the impedance given as

$$Z = \frac{\Delta V}{\Delta I} \tag{3}$$

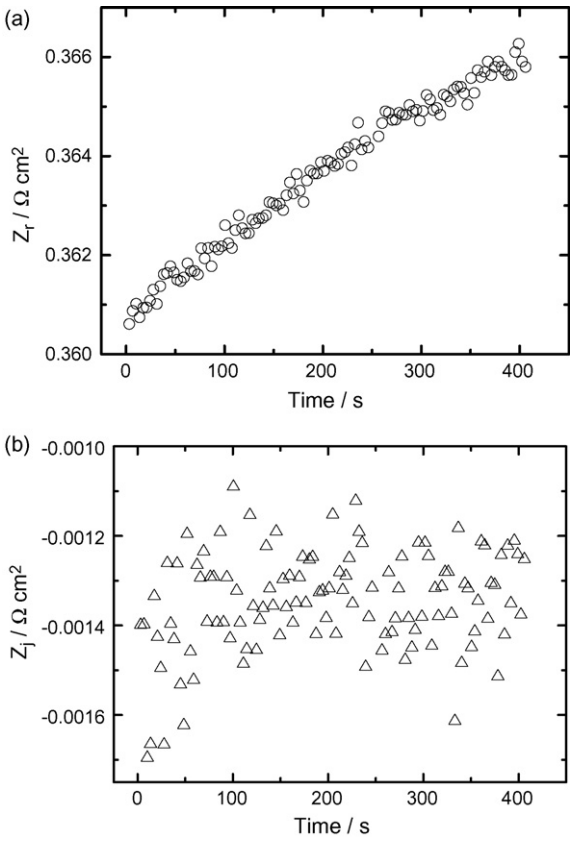

Fig. 7. Impedance measurement recorded at 0.4 A cm^{-2} and 1 Hz as functions of time at 70 °C: (a) real part; (b) imaginary part.

Eq. (2) can be written as

$$\sigma_Z^2 \cong \sigma_I^2 \left[\frac{\Delta V}{\Delta I^2}\right]^2 + \sigma_V^2 \left[\frac{1}{\Delta I}\right]^2 \tag{4}$$

or

$$\sigma_Z^2 \cong \frac{\sigma_I^2}{\Delta I^2} Z^2 + \sigma_V^2 \left[\frac{1}{\Delta I}\right]^2 \tag{5}$$

For galvanostatic modulation at fixed amplitude, Eq. (5) takes the form:

$$\sigma_Z \cong B|Z| + C \tag{6}$$

where C and B are constants.

The error structure model described by Eq. (1) is empirical and provided a better representation of the experimental error structure than did Eq. (6). The error structure is dependent on instrumental parameter settings which are not accounted for in the development of Eq. (6). While the above development did not yield the best model for the error structure, it serves to show that a dependence greater than first order on the impedance value is not expected.

The error structure identified for impedance spectra can be compared to that obtained for single-frequency transient measurements such as presented in Fig. 7 for impedance data collected at 0.4 A cm^{-2} and 1 Hz. The standard deviations for the real and imaginary parts of the impedance response are presented in Fig. 8(a) for a measured frequency of 100 Hz and in Fig. 8(b) for a frequency of 1 Hz. The error structure model represented by Eq. (1) is in good agreement with the standard deviations obtained by transient single-frequency measurements. At 100 Hz, Fig. 8(a), the standard deviation of the real and imaginary parts of the impedance

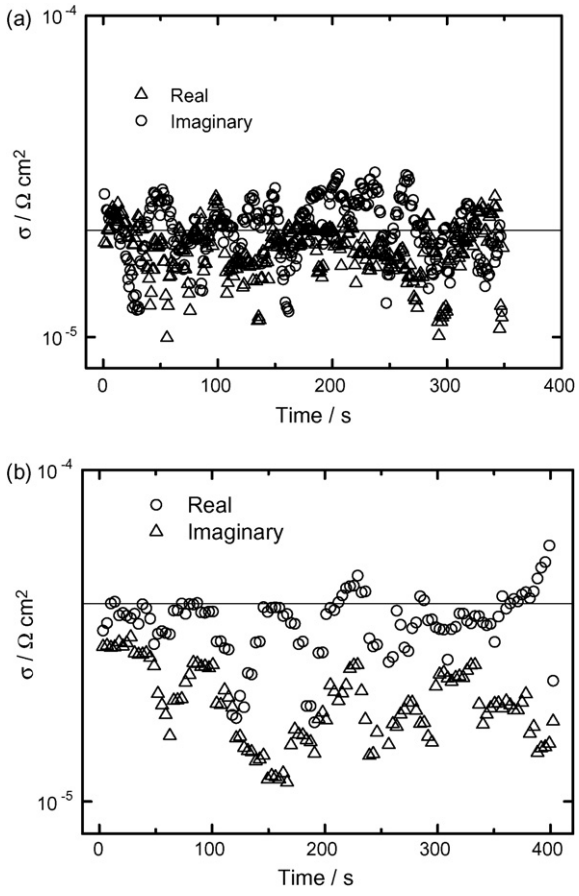

Fig. 8. The standard deviation of the single-frequency impedance measurements recorded at 0.4 A cm^{-2} and 70 ° C as functions of time: (a) at a frequency of 100 Hz; (b) at a frequency of 1 Hz (as presented in Fig. 7). The solid line represents the empirical model developed for the error structure given by Eq. (1).

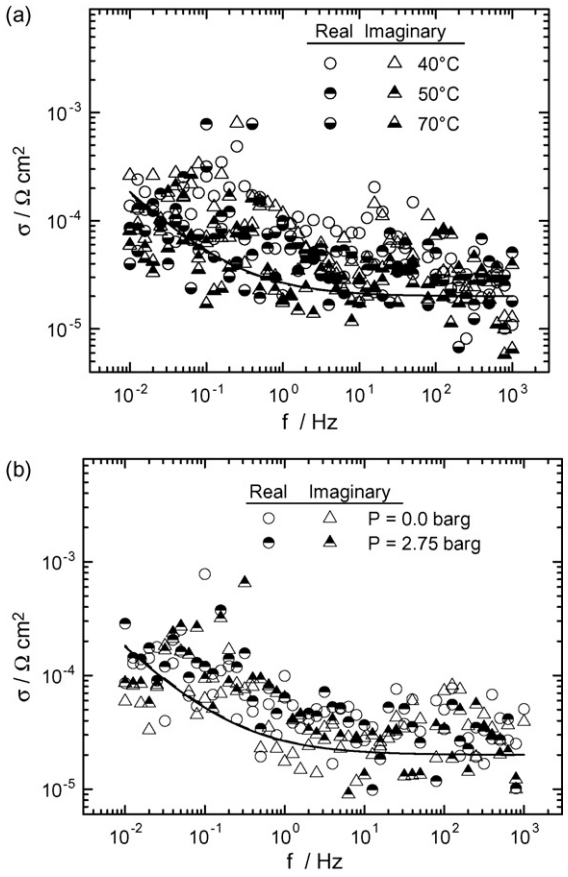

Fig. 9. Standard deviations for the impedance data obtained at a current density of 0.4 A cm^{-2}: (a) with system temperature as a parameter; (b) at 70 ° C with anode/cathode back-pressure as a parameter. The solid line represents the empirical model for the error structure given by Eq. (1).

are equal; however, as shown in Fig. 8(b), the standard deviations for real and imaginary parts are not equal at a frequency of 1 Hz. This result suggests that, even at a current density of 0.4 A cm^{-2}, where the error structure was the smallest, some flooding may be taking place.

Eq. (1) provided a good representation of the impedance error structure obtained at a current density of 0.4 A cm^{-2} under a broad variety of conditions. The error structure for the impedance response collected at different temperatures is presented in Fig. 9(a) and the influence of anode/cathode back-pressure is explored in Fig. 9(b). The model provided a good representation of the error structure for all cases considered in Fig. 9. Accordingly, Eq. (1) was used to represent the base-level standard deviation for measurements unaffected by drying or flooding conditions.

3.2.3. Detection of flooded conditions

Impedance spectra were obtained at different current densities. The standard deviations obtained at larger current densities are compared in Fig. 10 to the values obtained at 0.4 A cm^{-2}. The standard deviations obtained for current densities of 1.0 and 1.4 A cm^{-2} are clearly larger than that predicted by Eq. (1). The discrepancy may be attributed to stochastic processes within the cell such as associated with flooding.

The standard deviations presented in Fig. 5 were normalized by the base-stochastic errors level calculated using the error structure presented by Eq. (1). The result for the real part of the impedance is presented in Fig. 11. As shown in Fig. 11, the standard deviation of the impedance data increased with an increase in the operating current. The increased noise levels are seen at a frequency of 100 Hz as well as at lower frequencies. The normalized standard deviations for low current densities have some values less than unity, which may be attributed to uncertainty in the model for the baseline error structure due to the inability to avoid flooding completely in the data used to assess the baseline error structure. At large current densities and at low frequencies, the standard deviation calculated

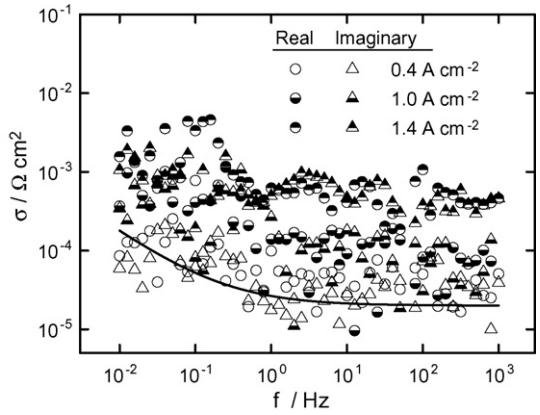

Fig. 10. Standard deviations for the impedance data obtained at a current densities of 0.4, 1.0, and 1.4 A cm^{-2}. The solid line represents the empirical model for the error structure given by Eq. (1).

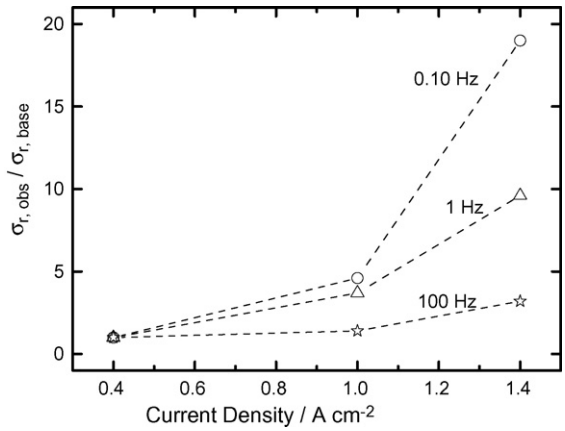

Fig. 11. Normalized standard deviations for the real part of the impedance calculated from the data shown in Fig. 3 as a function of current density with frequency as a parameter.

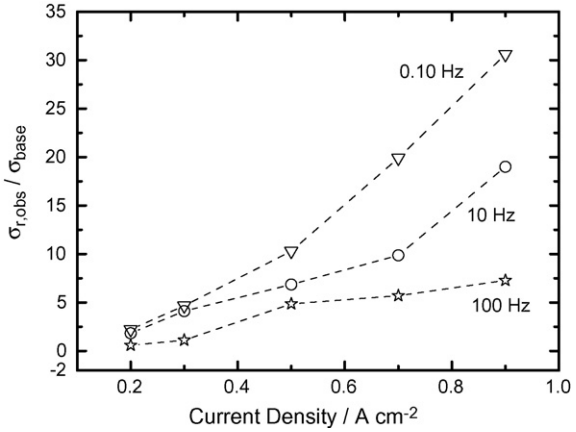

Fig. 13. Normalized standard deviations for the real part of the impedance as a function of current density with frequency as a parameter for the MEA with a uniform pore distribution. The anode, the cathode, and cell temperatures were set at 50 °C.

for the real part of the impedance was more than 20 times that obtained in the absence of flooding. The standard deviation of the imaginary part of the impedance had no clear dependency on flooding. The standard deviation of the real part particularly at low frequency, however, can be used to detect onset of flooding.

Similar experiments and analysis were performed on the MEA with a uniform GDL. The impedance response is presented in Fig. 12 with current density as a parameter. The scattering at higher current densities was more evident than observed for experiments using the non-uniform GDL. Transient single-frequency impedance measurements were used to obtain the standard deviations for real and imaginary parts of the impedance. The standard deviation for the real part of the impedance is presented in Fig. 13 as a function of current density for frequencies of 0.1, 10, and 100 Hz. The baseline error structure model used to normalize the data was calculated at a current density of 0.2 A cm^{-2}.

3.2.4. Detection of dry conditions

The stochastic errors for small current densities are shown in Fig. 14 for the MEA with a non-uniform pore distribution. The empirical model given by Eq. (1) provided a good description for the behavior at a current density of 0.4 A cm^{-2}, but the observed errors are much larger for lower current densities where dry conditions are anticipated. This result is consistent with the experimental observations of Schneider et al. [12] who report impedance scans with large scatter at low frequencies for dry conditions. Scatter observed for poorly humidified gas flows has been attributed in the literature to the appearance of multiple steady states [27,28]. In the present case, however, properly calibrated humidification bottles were to used to humidify the gas flows. The drying at low current densities can be attributed to reduced production of water at the cathode coupled with redistribution by electro-osmosis. This work shows that the standard deviation of the real part particularly at low frequency, however, can be used as well to detect the presence of dry conditions.

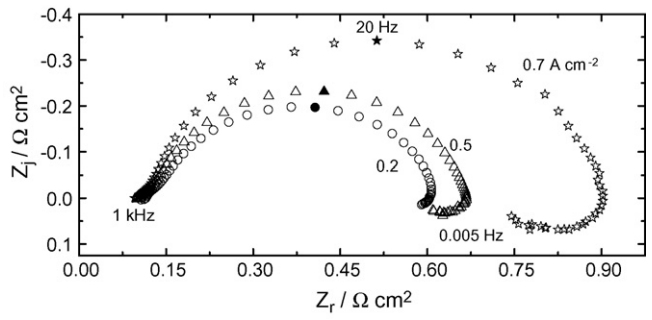

Fig. 12. The impedance data recorded using the MEA with a uniform GDL. The anode, the cathode, and cell temperatures were set at 50 °C.

4. Discussion

Due to its influence on mass transfer and kinetics, the onset of flooding in the fuel cell can be identified by a decrease in cell potential at fixed current or a decrease in current at fixed potential. Similarly, the onset of flooding can be identified by an increase in the cell impedance. In the present work, the increase in the low-frequency cell impedance associated with flooding was on the order of 20%. The increase of 20% in the cell impedance was accompanied by an increase in the standard deviation of the real part of the impedance by 2000 or 3000%.

The increase in stochastic errors in the impedance measurement can be attributed to the random character of the flooding process in which droplets of water are formed and then removed by gas flow. In fact, the increase in stochastic errors provides verification that the increased cell impedance was at least partially due to flooding. Impedance spectroscopy has been shown to provide a more sensi-

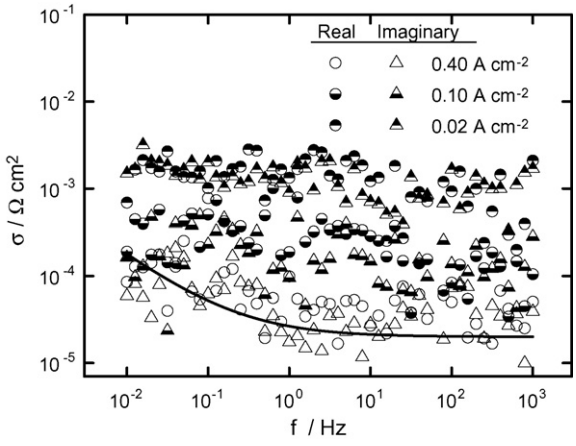

Fig. 14. Standard deviations for the impedance data obtained at a current densities of 0.02, 0.1, and 0.4 A cm^{-2}. The solid line represents the empirical model for the error structure given by Eq. (1). The anode, the cathode, and cell temperatures were set at 70 °C.

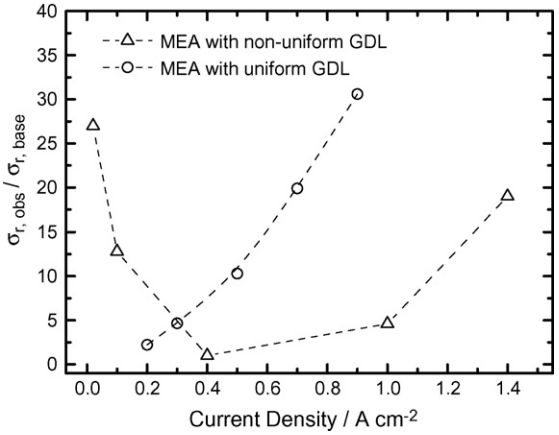

Fig. 15. Normalized standard deviations for the real part of the impedance measured at 0.1 Hz for fuel cells containing two different MEAs as a function of current density. The experiments for the uniform MEA were performed at 50 °C, and the experiments for the non-uniform MEA were performed at 70 °C.

tive assessment of cell condition than steady-state measurements of cell potential and current. The difficulty with using impedance directly to detect flooding is that a baseline value for the impedance must be established in the absence of flooding. This baseline must, however, change with time due to systematic changes to catalyst and membrane properties that are not associated with flooding. Thus, a baseline established when a cell is first commissioned will not be valid throughout the lifetime of the cell.

In contrast, the model given by Eq. (1) for the standard deviation of the impedance should be affected largely by instrumental settings, and, so long as the impedance is measured in the same way, a baseline established for the standard deviation of impedance measurements in the flooded condition should be valid throughout the lifetime of the cell. In addition, the change in the standard deviation of the measurement caused by flooding is 100 times larger than the corresponding change in the value of the impedance. Thus, assessment of the standard deviation of impedance measurements will provide a more sensitive indicator for the onset of flooding in a PEM fuel cell.

The standard deviation of the impedance measurements were sensitive to the properties of the MEA used in the experiment. A comparison of the normalized standard deviations for the real part of the impedance is presented in Fig. 15 with GDL properties as a parameter. The experiments for the uniform MEA were performed at 50 °C, and the experiments for the non-uniform MEA were performed at 70 °C. The normalized standard deviation increased at lower current densities for the GDL with a uniform pore distribution. The value was closer to unity over a broader range for the GDL with a non-uniform pore distribution. The results are consistent with the observation that a larger maximum current density could be obtained with the non-uniform GDL. Micro–macro-porous GDLs are reported to provide better water management [21–23]. The increase in normalized standard deviation at low current densities observed for the non-uniform GDL is likely due to drying of the membrane [7,9]. Similar experiments were not performed for the uniform GDL.

5. Conclusions

The flooding of gas diffusion layer pores in the fuel cell has been associated with increases in the internal cell resistance and in the impedance response of the fuel cell. The formation and removal of water droplets is an inherently stochastic process which increases the stochastic errors observed in impedance measurements. A measurement technique oriented towards assessment of the stochastic errors can therefore be used to identify the onset of flooding. In the present work, impedance spectroscopy was coupled with a measurement-model-based error analysis to detect onset of flooding. This method is particularly attractive because it is extremely sensitive and a well-defined baseline stochastic error can be established for the non-flooding condition.

The onset of flooding was examined for a 5 cm^2PEM fuel cell with an interdigitated flow channel. At low-current densities, the ratio of the observed standard deviation to the expected non-flooded standard deviation was close to unity. At larger current densities, the ratio for the real part of the impedance became quite large, with onset of flooding evident at current densities above 1 A cm^{-2} for the MEA with a non-uniform GDL and at current densities above 0.3 A cm^{-2} for the MEA with a uniform GDL. Drying was evident at current densities below 0.3 A cm^{-2} for the MEA with a non-uniform GDL.

The work presented here demonstrates that the stochastic error structure of impedance measurements may be used to detect operating conditions of the fuel cell which induce flooding or drying. In this case, the flooding or drying phenomena contribute stochastic errors which are superposed on those associated with the electronic instrumentation. As shown in the present work, onset of flooding is gradual and can be affected by factors such as flow channel design and GDL characteristics. The current density reported in the present work for onset of flooding may be useful for the systems investigated here, but the approach is general and can be exploited to evaluate flooding and drying characteristics for larger fuel cells and for other cell designs. The next step in the development of this technique would be to couple the impedance error analysis approach with methods for direct measurement of liquid water in the fuel cell such as neutron imaging [12] or the residence time distribution technique [29,30].

Acknowledgements

This work was supported by NASA Glenn Research Center under grant NAG 3-2930 monitored by Timothy Smith with additional support from Gamry Instruments Inc. The Department of Chemical Engineering, University of Florida assisted in meeting the publication costs of this article.

References

[1] A.A. Kulikovsky, J. Electrochem. Soc. 150 (11) (2003) A1432–A1439.
[2] P. Berg, K. Promislow, J.S. Pierre, J. Stumper, B. Wetton, J. Electrochem. Soc. 151 (3) (2004) A341–A353.
[3] A. Su, F. Weng, C. Hsu, Y. Chen, Int. J. Hydrogen Energy (2006) 1031–1039.
[4] J. St-Pierre, J. Electrochem. Soc. 154 (7) (2007) B724–B731.
[5] W. He, J.S. Yi, T.V. Nguyen, AIChE 46 (10) (2000) 2053–2064.
[6] S.W. Cha, R. Hayre, Y. Park, F.B. Prinz, J. Power Sources 161 (2006) 138–142.
[7] F. Barbir, H. Gorgun, X. Wang, J. Power Sources 141 (2005) 96–101.
[8] S. Ge, C.-Y. Wang, J. Electrochem. Soc. 154 (10) (2007) B998–B1005.
[9] J.-M. LeCanut, R.M. Abouatallah, D.A. Harrington, J. Electrochem. Soc. 153 (2006) A857–A864.
[10] W. Merida, D.A. Harrington, J.-M. LeCanut, G. McLean, J. Power Sources 161 (2006) 264–274.
[11] I.A. Schneider, H. Kuhn, A. Wokaun, G.G. Scherer, J. Electrochem. Soc. 152 (10) (2005) A2092–A2103.
[12] I.A. Schneider, H. Kuhn, A. Wokaun, G.G. Scherer, Electrochem. Commun. 7 (2005) 1393–1397.
[13] I.A. Schneider, H. Kuhn, A. Wokaun, G.G. Scherer, J. Electrochem. Soc. 152 (12) (2005) A2383–A2389.
[14] N. Fouquet, C. Doulet, C. Nouillant, G. Dauphin-Tanguy, B. Ould-Bouamama, J. Power Sources 159 (2006) 905–913.
[15] P. Agarwal, M.E. Orazem, L.H. García-Rubio, J. Electrochem. Soc. 139 (7) (1992) 1917–1927.
[16] P. Agarwal, O.D. Crisalle, M.E. Orazem, L.H. García-Rubio, J. Electrochem. Soc. 142 (1995) 4149–4158.
[17] P. Agarwal, M.E. Orazem, L.H. García-Rubio, J. Electrochem. Soc. 142 (1995) 4156–4159.

[18] M.E. Orazem, J. Electroanal. Chem. 572 (2004) 317–327.
[19] S.K. Roy, M.E. Orazem, J. Electrochem. Soc. 154 (8) (2007) B883–B891.
[20] S.K. Roy, M.E. Orazem, ECS Trans. 11 (1) (2007) 485–495.
[21] T.E. Springer, T.A. Zawodzinski, M.S. Wilson, S. Gottesfeld, J. Electrochem. Soc. 143 (1996) 587–599.
[22] V.A. Paganin, C.L.F. Oliveira, E.A. Ticianelli, T.E. Springer, E.R. Gonzalez, Electochim. Acta 43 (1998) 3761–3766.
[23] W.K. Lee, C.-H. Ho, J.W.V. Zee, M. Murthy, J. Power Sources 84 (1999) 45–51.
[24] M. Durbha, M.E. Orazem, L.H. García-Rubio, J. Electrochem. Soc. 144 (1997) 48–55.
[25] M.E. Orazem, P. Agarwal, C. Deslouis, B. Tribollet, J. Electrochem. Soc. 143 (1996) 948–960.
[26] M.E. Orazem, T.E. Moustafid, C. Deslouis, B. Tribollet, J. Electrochem. Soc. 143 (1996) 3880–3890.
[27] R. Hanke-Rauschenbach, M. Mangold, K. Sundmachera, J. Electrochem. Soc. 155 (2) (2008) B97–B107.
[28] I. Nazarov, K. Promislow, Chem. Eng. Sci. 61 (2006) 3198–3209.
[29] J. St-Pierre, A. Wonga, J. Diep, D. Kiel, J. Power Sources 164 (1) (2007) 196–202.
[30] J. Diep, D. Kiel, J. St-Pierre, A. Wong, Chem. Eng. Sci. 62 (2007) 846–857.